The Eighteenth International Symposium on Artificial Life and Robotics 2013 (AROB 18th '13),
Daejeon Convention Center, Daejeon, Korea, January 30-February 1, 2013

Modeling and robust decoupling control for hypersonic scramjet vehicle

Xiaofeng Su[1], Yuefei Jiang[1], Yingmin Jia[1,2]

[1] The Seventh Research Division and the Department of Systems and Control, Beihang University (BUAA),
Beijing 100191, China (e-mail: xfsu@smss.buaa.edu.cn; jyf1214@126.com).
[2] Key Laboratory of Mathematics, Informatics and Behavioral Semantics (LMIB), SMSS, Beihang University (BUAA),
Beijing 100191, China (e-mail: ymjia@buaa.edu.cn).

Abstract: In this paper, the modeling and the robust decoupling control for a generic hypersonic scramjet vehicle are studied. Firstly, the dynamics of the hypersonic vehicle are modeled by applying the Lagrangian approach, which captures the most primary characteristics such as elastic deformation, aerodynamics, aero-heating, variable mass, effect of spherical rotating earth and their inherent interactions. Then, a robust output decoupling controller is designed by using nonlinear dynamic inversion plus the desired proportional integral dynamics, and natural time-scale separation theorem between fast and slow variables. Finally, the nonlinear simulations demonstrate that the controller can eliminate the interaction among the output channels and satisfy the handling quality requirements when the vehicle has parameter uncertainty.

Keywords: HSV modeling, robust output decoupling, dynamic inversion, multitime-scale approach

1 INTRODUCTION

With the historic scramjet-powered Mach 7 and 10 flights of the X-43A in 2004, the research of hypersonic scramjet vehicle (HSV) has seen a resurgence within the aerospace community. This is attributed to the fact that the HSV is viewed as the next critical flying vehicle, which has the ability to easily penetrate and survive against enemy air defenses, promptly reach critical targets at long ranges (i.e., realize rapid global response), and access to space in a manner similar to commercial air travel. Therefore, on one hand, this type of vehicle has great potential as a high-speed, time-saving, and low-cost transport for both commercial and military applications. On the other hand, the modeling and control of the HSV are challenging, due to its severe aero-heating, unconventional propulsion system, much broader flight envelope, and tight interaction among airframe, propulsion, and structure [1, 2].

The modern HSV like NASA X-43 or X-51 has special slender airframe-propulsion lifting-body configuration and operates over a high speed ranging from Mach 5 to Mach 15 within large flight envelope, so that the traditional design approaches are invalid when there exist the manifold interaction among sub-models of the HSV and the complex flight environment. For the modeling issue, several literature [3, 4, 5] have discussed the determinants of the modeling and the interaction of the sub-models. In [3, 4], the inertial dynamics of the model were obtained under the consideration of rigid-body motion, elastic deformation and spherical rotating earth. And McNamara et al [5] focused on the coupling effects among the sub-models of aerodynamics, aero-elasticity and aero-heating based on high fidelity codes. For the decoupling control issue, nonlinear dynamic inversion control method was used in [6, 7] under the condition that the system dynamics were exactly known. Moreover, the stability and performance robustness within the dynamic inversion framework were addressed in [8, 9, 10].

In this work, because of the high computational requirements when applying the precise sub-models of the HSV, some dominating elements and their primary interactions are extracted in the process of modeling. And then, by utilizing the Lagrangian approach, a control-oriented model of the HSV is obtained, in which the effects of inertial dynamics, elastic deformation, aerodynamics, aero-heating, variable mass, and spherical rotating earth are captured. Based on this model, a robust output decoupling controller is designed to enhance the maneuverability of the HSV. Specifically, the dynamics of the vehicle are separated into two time scales according to the natural time-scale separation theorem. In each time-scale loop, an appropriate proportional integral control law is designed in conjunction with the dynamic inversion controller, such that the outputs of the closed-loop system can be robustly decoupled at the steady state with respect to the parameter uncertainty.

2 VEHICLE MODEL

According to [11], the dynamical equations of the HSV are directly presented by using the Lagrangian approach.

$$m\dot{V} - \tilde{S}\dot{\omega} + \int_m \dot{v}dm = \left(\int_m \tilde{v}dm\right)\cdot\omega + mg + F + \Psi_F \quad (1)$$

$$\begin{aligned}\tilde{S}\dot{V} + J\dot{\omega} + \int_m \tilde{r}\dot{v}dm = &\left(2\int_m \tilde{r}\tilde{v}dm - \tilde{\omega}J\right)\cdot\omega \\ &- \left(\int_m \tilde{v}dm + \tilde{\omega}\tilde{S}\right)\cdot V + \bar{M} + \Psi_{\bar{M}}\end{aligned} \quad (2)$$

$$[\Lambda]\dot{V}+[\Lambda]\tilde{r}^T\dot{\omega}+[\Lambda]\dot{v}=[\Lambda]\tilde{V}\omega-[\Lambda]\tilde{\omega}\tilde{\omega}r - \int_m\left(\phi_i^2\bar{\omega}_i^2\eta_i\right)dm+Q_e+\Psi_e. \tag{3}$$

The expressions of external forces, moments, and thrust in (1), (2), (3) are extremely complicated, which are determined not only by the velocity and the attitude, but also by the shape and elastic deformation of the HSV. In summary, there are $12+3n$ (n is the number of elastic modes) equations such as: 3 force equations, 3 moment equations, $3n$ elastic deformation equations, 3 trajectory equations, and 3 Euler angle equations. Moreover, the kinematic equations of the HSV are similar as the ones of the regular vehicle. For a vehicle flying over a Mach number ranging from 5 to 15 and a height ranging from 20 to $60km$, the maximum and minimum magnitudes of the Coriolis force $m\omega_{E,I}\times V_r$ are approximately 7.02% and 2.48% of the vehicle weight, and the magnitude of the transport force $m\omega_{E,I}\times(\omega_{E,I}\times R)$ is about 0.35% of the vehicle weight. Finally, the scalar form of the HSV model which is used here are presented in Appendix based on three regular assumptions: i) neglecting the effect of elastic deformation , ii) neglecting the transport item in expression of $\dot{V}$, iii) the vehicle is symmetrical about the ox_Bz_B plane.

3 ROBUST DECOUPLING CONTROLLER

The structure of resulting control law is shown in Fig. 1., in which the nonlinear dynamic inversion theory is applied in two time scales. Because the integral feedback has the ability of eliminating steady-state errors, a desired dynamic (i.e., proportional plus integral feedback dynamic) is applied to solve the robustness problem of the dynamic inversion.

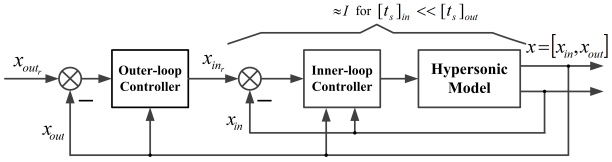

Fig. 1. Two-time scale feedback loop

3.1 Outer-loop Controller design

In the outer loop, the nominal dynamics of slow time scale are placed in the form of (4). The objective of the dynamic inversion in the slow time scale is to realize the decoupling control of the attitude angles and flight trajectory using the rotational rate and flight velocity. And the outputs are chosen to be the system states.

$$\dot{\mathbf{x}}_{out}=\tilde{F}^0(\mathbf{x}_{out})+\tilde{G}^0(\mathbf{x}_{out})\cdot\mathbf{x}_{in} \tag{4}$$

where $\mathbf{x}_{out}=[\phi\ \ \theta\ \ \psi\ \ x\ \ y\ \ -h]^T=\mathbf{y}_{out}$, $\mathbf{x}_{in}=[\omega_x\ \omega_y\ \omega_z\ u\ v\ w]^T$. Roll angel ϕ, pitch angle θ, yaw angle ψ are the attitude angels of the body axes relative to the earth axes. x,y are flight displacement along the longitude lines and latitude lines, respectively. h is the altitude of the vehicle. ω_x, ω_y, ω_z are rotational rates of the body axes relative to the inertial axes. u, v, w are the velocities along the body axes related to the earth axes. In practice, because of the parameter uncertainties, the real system is presented as

$$\dot{\mathbf{x}}_{out}=\tilde{F}(\mathbf{x}_{out})+\tilde{G}(\mathbf{x}_{out})\cdot\mathbf{x}_{in} \tag{5}$$

where $\tilde{F}(\mathbf{x}_{out})=\tilde{F}^0(\mathbf{x}_{out})+\Delta\tilde{F}(\mathbf{x}_{out})$, $\tilde{G}(\mathbf{x}_{out})=\tilde{G}^0(\mathbf{x}_{out})+\Delta\tilde{G}(\mathbf{x}_{out})$. And the specific expressions of $\tilde{F}(\mathbf{x}_{out})$, $\tilde{F}^0(\mathbf{x}_{out})$, $\tilde{G}(\mathbf{x}_{out})$, and $\tilde{G}^0(\mathbf{x}_{out})$ can be obtained from the Euler angle equations and the trajectory equations. Moreover, the parameter uncertainties in these expressions have the forms as $\omega_E=\omega_E^0+\Delta\omega_E$, $R_E=R_E^0+\Delta R_E$, and $\lambda_0=\lambda_0^0+\Delta\lambda_0$.

Since the total relative degree is equal to the number of system states, this time scale has no internal dynamics to be considered. Then, the outer-loop control law is given by (6), where the desired dynamics is chosen to have the proportional integral form.

$$\begin{cases}\mathbf{x}_{in}=[\tilde{G}^0(\mathbf{x}_{out})]^{-1}\left\{-[\tilde{F}^0(\mathbf{x}_{out})]+\mathbf{v}_{des}\right\}\\ \mathbf{v}_{des}=\mathbf{k}_{out\_1}\cdot(\mathbf{v}_{out}-\mathbf{x}_{out})+\mathbf{k}_{out\_2}\cdot\Omega\\ \dot{\Omega}=\mathbf{v}_{out}-\mathbf{x}_{out}\end{cases} \tag{6}$$

where $\Omega=[\Omega_\phi\ \ \Omega_\theta\ \ \Omega_\psi\ \ \Omega_x\ \ \Omega_y\ \ \Omega_h]^T$. $\mathbf{k}_{out\_i}=[k_{out\_\phi i}\ k_{out\_\theta i}\ k_{out\_\psi i}\ k_{out\_xi}\ k_{out\_yi}\ k_{out\_hi}]^T$, $i=1,2$ are the desired controller parameters which will be determined. $\mathbf{v}_{out}=[v_\phi\ v_\theta\ v_\psi\ v_x\ v_y\ v_h]^T$ is the virtual input vector. By calculating the determinant of the control matrix $det[\tilde{G}^0(\mathbf{x}_{out})]$, it is concluded that $[\tilde{G}^0(\mathbf{x}_{out})]^{-1}$ exists while the inequality $1/\cos\theta\neq 0$ holds, and it is obviously satisfied.

Substituting the control law (6) into the real system (5), the outer closed-loop system is obtained. Then, the objective is to find the appropriate controller parameters $\mathbf{k}_{out\_1}$ and $\mathbf{k}_{out\_2}$, so that the equation $\mathbf{y}_{out}=[\ \mathbf{I}\ ]\mathbf{v}_{out}$ (i.e., $\mathbf{x}_{out}=[\ \mathbf{I}\ ]\mathbf{v}_{out}$, where $[\ \mathbf{I}\ ]$ is the identity matrix) is satisfied at the steady state while the system contains parameter uncertainties. Next, setting $\dot{\mathbf{x}}_{out}=\dot{\Omega}=0$ yields the equilibrium solutions of this system: $\mathbf{x}_{out_e}=\mathbf{v}_{out}$, $\Omega_e=[-\Delta\tilde{f}_1/k_{out\_\phi 2}\ -\Delta\tilde{f}_2/k_{out\_\theta 2}\ -\Delta\tilde{f}_3/k_{out\_\psi 2}\ 0\ 0\ 0]^T$. Linearizing about $\mathbf{x}_{out}=\mathbf{x}_{out_e}$ and $\Omega=\Omega_e$ yields the following linear systems: $\Delta\dot{\mathbf{x}}_{out}=[\tilde{A}]_{6\times 6}\cdot\Delta\mathbf{x}_{out}+[\tilde{B}]_{6\times 6}\cdot\Delta\Omega$, $\Delta\dot{\Omega}=[\tilde{C}]_{6\times 6}\cdot\Delta\mathbf{x}_{out}+[\tilde{D}]_{6\times 6}\cdot\Delta\Omega$. Then, the characteristic equation of such a linear system is:

$$s^{12}+\tilde{n}_{11}s^{11}+\tilde{n}_{10}s^{10}+\cdots+\tilde{n}_1s^1+\tilde{n}_0=0$$

where $\tilde{n}_i=\tilde{n}_i(\mathbf{v}_{out},\mathbf{k}_{out\_1},\mathbf{k}_{out\_2},\Delta)$, $i=0,\cdots,11$. Hence, the stability of that linear system is guaranteed, if the eigenvalues of the characteristic equation are less than zero for all allowable $\Delta\tilde{F}$ and $\Delta\tilde{G}$. Moreover, desirable stability margin can be obtained for better dynamic performance by substituting a new variable $s_1=s+a$ into the original characteristic equation. Therefore, the linear system is stable and the eigenvalues are on the left side of the axis $s=-a$.

3.2 Inner-loop Controller design

In the inner loop, the control surfaces and vectored thrust are commanded to realize prompt and precise tracking of the flight velocity and rotational angular velocity generated in the outer loop. The most important point is that the slow time scale states in the outer loop are treated as constants in this fast time scale, since they evolve more slowly when compared with fast time scale ones. The real system dynamics of fast time scale are written as

$$\dot{\mathbf{x}}_{in} = F(\mathbf{x}) + G(\mathbf{x}) \cdot \mathbf{u} \tag{7}$$

and $F(\mathbf{x}) = F^0(\mathbf{x}) + \Delta F(\mathbf{x})$, $G(\mathbf{x}) = G^0(\mathbf{x}) + \Delta G(\mathbf{x})$, $\mathbf{x}_{in} = [u\ v\ w\ \omega_x\ \omega_y\ \omega_z]^T$, $\mathbf{u} = [\Phi_x\ \Phi_y\ \Phi_z\ \delta_e\ \delta_a\ \delta_r]^T$. The system states $\mathbf{x}_{in}$ are the same as ones in the outer loop, and $\mathbf{x} = [\mathbf{x}_{in}^T,\ \mathbf{x}_{out}^T]$. The three control surfaces deflection δ_e, δ_a, δ_r are the effective elevator, aileron and rudder deflection. Throttle setting values Φ_x, Φ_y, Φ_z are used to generate vectored thrust. Besides, according to the force equations and moment equations, the expressions of $F(\mathbf{x})$, $F^0(\mathbf{x})$, $G(\mathbf{x})$, and $G^0(\mathbf{x})$ can be obtained. The parameter uncertainties exist not only in ω_E, R_E, λ_0, but also in vehicle mass, moment of inertia, product of inertia, aerodynamic derivatives, and thrust derivatives. Similarly, the desired dynamics of the fast time scale also have proportional integral form, thus inner-loop control law is written as

$$\begin{cases} \mathbf{u} = [G^0(\mathbf{x})]^{-1} \left\{ -[F^0(\mathbf{x})] + \mathbf{k}_{in\_1} \cdot (\mathbf{x}_{in_r} - \mathbf{x}_{in}) + \mathbf{k}_{in\_2} \cdot \Omega \right\} \\ \dot{\Omega} = \mathbf{x}_{in_r} - \mathbf{x}_{in} \end{cases} \tag{8}$$

where $\Omega = [\Omega_u\ \ \Omega_v\ \ \Omega_w\ \ \Omega_{\omega_x}\ \ \Omega_{\omega_y}\ \ \Omega_{\omega_z}]^T$. $\mathbf{k}_{in\_i} = [k_{in\_ui}\ k_{in\_vi}\ k_{in\_wi}\ k_{in\_\omega_x i}\ k_{in\_\omega_y i}\ k_{in\_\omega_z i}]^T$, $i = 1,2$ are the controller parameters to be designed. Besides, matrix $[G^0(\mathbf{x})]^{-1}$ exists if the following inequalities holds.

$$\begin{cases} \Psi^0_{F_x\_\Phi_x}(\mathbf{x}) \cdot \Psi^0_{F_y\_\Phi_y}(\mathbf{x}) \cdot \Psi^0_{F_z\_\Phi_z}(\mathbf{x}) \neq 0 \\ \bar{M}^0_{y\_\delta_e}(\mathbf{x}) \left[\bar{M}^0_{x\_\delta_r}(\mathbf{x}) \cdot \bar{M}^0_{z\_\delta_a}(\mathbf{x}) - \bar{M}^0_{x\_\delta_a}(\mathbf{x}) \cdot \bar{M}^0_{z\_\delta_r}(\mathbf{x}) \right] \neq 0 \end{cases}$$

Consequently, substituting the controller (8) into the real system (7) yields the inner closed-loop system. Next, get the equilibrium solutions of this closed-loop system by setting $\dot{\mathbf{x}}_{in} = \dot{\Omega} = 0$. Then linearizing about $\mathbf{x}_{in} = \mathbf{x}_{in_e} = \mathbf{x}_{in_r}$ and $\Omega = \Omega_e$ could yield corresponding linear systems: $\Delta\dot{\mathbf{x}}_{in} = [A]_{6\times6} \cdot \Delta\mathbf{x}_{in} + [B]_{6\times6} \cdot \Delta\Omega$, $\Delta\dot{\Omega} = [C]_{6\times6} \cdot \Delta\mathbf{x}_{in} + [D]_{6\times6} \cdot \Delta\Omega$. For the linear system above with uncertainties in ΔF and ΔG, the robust stability of that system is analogously achievable through finding suitable controller parameters $\mathbf{k}_{in\_i}(\mathbf{x}_{in_r})$, $i = 1,2$. Furthermore, the desirable stability margin can also be obtained for better dynamic performance.

Remark1: The nonlinear dynamic inversion method is a straight forward approach for designing decoupled feedback systems of nonlinear systems. For the system with parameter uncertainty, the robustness of output decoupling controller can be addressed by using integral terms within the loops.

Remark2: The information of $\mathbf{v}_{out}$ is required in the processing of determining decoupling controller parameters $\mathbf{k}_{out}(\mathbf{v}_{out})$. And this information can be easily obtained from the commands.

Remark3: The linearized model of the nonlinear system has been discussed here, which means that the states convergency can only be achieved in a neighborhood of the equilibrium. Fortunately, this problem can be solved by limiting the change rate of the commands or enhancing the response speed of the systems.

4 SIMULATION RESULTS

A typical nonlinear simulation of the maneuver is shown to examine the effectiveness of the robust output decoupling controller. The data of aerodynamic characteristics and thrust performance in [12] is adopted here. The simulation results of nonlinear system responses to the change of roll angel, velocity and altitude are depicted in Fig. $2-4$, in which the solid line is the response to $v1$ and the dash line is the response to $v2$. It is observed that the change of one output value has no effect on the steady-state values of the others.

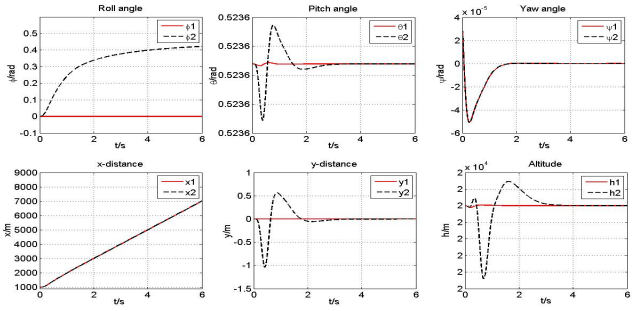

Fig. 2. Responses to the change of roll angle

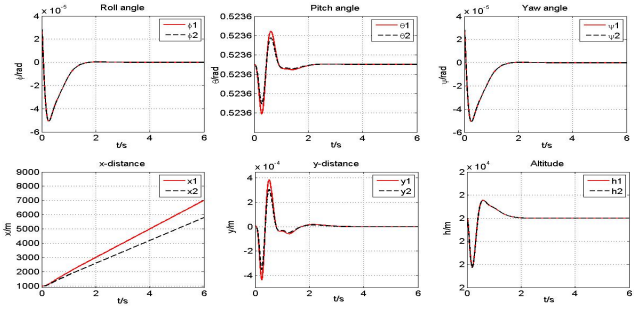

Fig. 3. Responses to the change of velocity

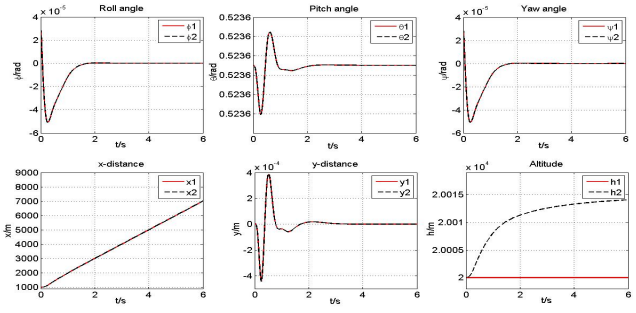

Fig. 4. Responses to the change of altitude

5 CONCLUSION

In this paper, a multivariable nonlinear strong-coupled HSV model has been developed, which captures the most primary characteristics of this special vehicle. Based on this model, a robust decoupling controller design method, which incorporates a desired proportional integral dynamic with nonlinear dynamic inversion controller, has been proposed. This controller design method mainly addresses two fundamental problems: decoupling of nonlinear system and decoupling robustness. The nonlinear simulation results confirm that the vehicle model equipped with the robust output decoupling controller can provide both steady-state decoupling of the outputs and robustness with respect to parameter uncertainty.

6 APPENDIX

Force equations:

$$\begin{aligned}
\dot{u} &= [\omega_z + \omega_E(T_{31}c\lambda - T_{33}s\lambda)]v \\
&\quad -[\omega_y + \omega_E(T_{21}c\lambda - T_{23}s\lambda]w + gT_{13} + (F_x + \Psi_{F_x})/m \\
\dot{v} &= [\omega_x + \omega_E(T_{11}c\lambda - T_{13}s\lambda)]w \\
&\quad -[\omega_z + \omega_E(T_{31}c\lambda - T_{33}s\lambda)]u + gT_{23} + (F_y + \Psi_{F_y})/m \\
\dot{w} &= [\omega_y + \omega_E(T_{21}c\lambda - T_{23}s\lambda)]u \\
&\quad -[\omega_x + \omega_E(T_{11}c\lambda - T_{13}s\lambda)]v + gT_{33} + (F_z + \Psi_{F_z})/m
\end{aligned}$$

Moment equations:

$$\begin{aligned}
J_{xx}\dot{\omega}_x - J_{xz}\dot{\omega}_z &= J_{xz}\omega_x\omega_y + (J_{yy} - J_{zz})\omega_y\omega_z + \bar{M}_x + \Psi_{\bar{M}_x} \\
J_{yy}\dot{\omega}_y &= (J_{zz} - J_{xx})\omega_x\omega_z + J_{xz}(\omega_z^2 - \omega_x^2) + \bar{M}_y + \Psi_{\bar{M}_y} \\
J_{zz}\dot{\omega}_z - J_{xz}\dot{\omega}_x &= -J_{xz}\omega_y\omega_z + (J_{xx} - J_{yy})\omega_x\omega_y + \bar{M}_z + \Psi_{\bar{M}_z}
\end{aligned}$$

Euler angle equations:

$$\begin{aligned}
\dot{\phi} &= \omega_x + (\omega_z c\phi + \omega_y s\phi)t\theta - (c\theta c\phi + s\theta c\phi t\theta)(v/R) \\
&\quad +(c\theta s\phi + s\theta s\phi t\theta)(w/R) - \omega_E(c\psi s\theta t\theta + c\psi c\theta)c\lambda \\
\dot{\theta} &= \omega_y c\phi - \omega_z s\phi + c\theta(u/R) + s\theta s\phi(v/R) + s\theta c\phi(w/R) \\
&\quad +\omega_E s\psi c\lambda \\
\dot{\psi} &= (1/c\theta)(\omega_z c\phi + \omega_y s\phi) - \omega_E(c\psi t\theta c\lambda - s\lambda) \\
&\quad +s\psi c\theta t\lambda(u/R) + [(s\psi s\theta s\phi + c\psi c\phi)t\lambda - c\phi t\theta](v/R) \\
&\quad +[(s\psi s\theta c\phi - c\psi s\phi)t\lambda + s\phi t\theta](w/R)
\end{aligned}$$

Trajectory equations:

$$\begin{aligned}
\dot{x} &= T_{11}u + T_{21}v + T_{31}w \\
\dot{y} &= T_{12}u + T_{22}v + T_{32}w \\
-\dot{h} &= T_{13}u + T_{23}v + T_{33}w
\end{aligned}$$

where $R = R_E + h$, $\lambda = \lambda_0 + x/R_E$, $s = \sin$, $c = \cos$, $t = \tan$,

$$[T_{ij}] = \begin{bmatrix} c\psi c\theta & s\psi c\theta & -s\theta \\ c\psi s\theta s\phi - s\psi c\phi & s\psi s\theta s\phi + c\psi c\phi & c\theta s\phi \\ c\psi s\theta c\phi + s\psi s\phi & s\psi s\theta c\phi - c\psi s\phi & c\theta c\phi \end{bmatrix}.$$

And u, v, w, ω_x, ω_y, ω_z, ϕ, θ, ψ, x, y, h are the system states. Input control variables are Φ_x, Φ_y, Φ_z, δ_e, δ_a, δ_r, which are included in the expressions of the force, moment and thrust.

7 ACKNOWLEDGMENTS

This work was supported by the National Basic Research Program of China (973 Program, 2012CB821200, 2012CB821201) and the NSFC (61134005, 60921001, 90916024, 91116016).

REFERENCES

[1] Kelkar AG, Vogel JM, Whitmer CE, and et al (2011), Design Tool for Control-Centric Modeling, Analysis, and Trade Studies for Hypersonic Vehicles. Proceedings of the 17th AIAA International Space Planes and Hypersonic Systems and Technologies Conference.

[2] Rodriguez AA, Dickeson JJ, Sridharan S, and et al (2009), Control-Relevant Modeling ,Analysis, and Design for Scramjet-Powered Hy-personic Vehicles. Proceedings of the16th AIAA/DLR/DGLR International Space Planes and Hypersonic Systems and Technologies Conference.

[3] Bilimoria KD and Schmidt DK (1995), Integrated Development of the Equations of Motion for Elastic Hypersonic Flight Vehicles. Journal of Guidance, Control, and Dynamics, 18(1): 73–81.

[4] Meirovitch L and Tuzcu I (2003), Integrated Approach to the Dynamics and Control of Maneuvering Flexible Aircraft. NASA/CR–2003–211748.

[5] McNamara J and Friedmann P (2011), Aeroelastic and Aerothermoelastic Analysis in Hypersonic Flow: Past, Present, and Future. AIAA Journal, 49(6): 1089–1122.

[6] Snell SA (1998), Decoupling Control Design with Applications to Flight. Journal of Guidance, Control, and Dynamics, 21(4): 647–655.

[7] Bajodah AH (2009), Generalised dynamic inversion spacecraft control design methodologies. IET Control Theory and Applicaions, 3(2): 239–251.

[8] Reiner J, Balas GJ, and Garrard WL (1996), Flight Control Design Using Robust Dynamic Inversion and Time-scale Separation. Automatica, 32(11): 1493–1504.

[9] Ito D and Valasek J (2001), Robust Dynamic Inversion Controller Design and Analysis for the X-38. AIAA Guidance, Navigation and Control Conference.

[10] Georgie J and Valasek J (2003), Evaluation of Longitudinal Desired Dynamics for Dynamic-Inversion Controlled Generic Reentry Vehicles. Journal of Guidance, Control, and Dynamics, 26(5): 811–819.

[11] Su XF, Jia YM, Du JP, and et al (2012), Integrated Approach to Hypersonic Vehicle Modeling. Proceedings of the 31th Chinese Control Conference, pp. 1752–1758.

[12] Li HF, Lin P, and Xu DJ (2011), Control-oriented Modeling for Air-breathing Hypersonic Vehicle Using Parameterized Configuration Approach. Chinese Journal of Aeronautics, 24: 81–89.